Coherent optical generation of nonequilibrium electrons studied via band-to-acceptor luminescence in GaAs

Alfred Leitenstorfer
Physik Department E 11, Technische Universität München, D-85748 Garching, Germany

Thomas Elsaesser
Max-Born-Institut für Nichtlineare Optik und Kurzzeitspektroskopie, D-12489 Berlin, Germany

Fausto Rossi
Fachbereich Physik, Philipps-Universität Marburg, D-35032 Marburg, Germany

Tilmann Kuhn
Lehrstuhl für Theoretische Physik, Brandenburgische Technische Universität, D-03013 Cottbus, Germany

W. Klein, G. Boehm, G. Traenkle, and G. Weimann
Walter-Schottky-Institut, Technische Universität München, D-85748 Garching, Germany
(Received 1 September 1995)

Nonequilibrium electrons generated by coherent optical excitation of GaAs are studied in a wide range of carrier density. The electron distribution is monitored via spectrally resolved band-to-acceptor luminescence after continuous-wave, picosecond, or femtosecond laser excitation. Our data demonstrate that the coherent coupling between the laser radiation and the interband polarization and its dephasing strongly influence the initial carrier distribution. The energetic width of carrier generation is broadened due to rapid phase-breaking scattering events during carrier generation. Theoretical results from a Monte Carlo solution of the semiconductor Bloch equations including on the same kinetic level coherent and incoherent phenomena show that the broadening of the electron distribution is introduced mainly in the generation process whereas the recombination of electrons with bound holes makes a minor contribution. The theoretical results are in quantitative agreement with the experimental data.

I. INTRODUCTION

The nonequilibrium dynamics of electrons and holes are governed by the coupled elementary excitations of the carrier system and of the lattice and occur frequently on subpicosecond time scales. Optical spectroscopy with ultrashort laser pulses provides direct information on such phenomena and has allowed the distinguishing between the coherent and incoherent dynamics of carriers.[1] At early times during excitation, the laser pulse creates a polarization of the semiconductor that couples coherently to the electric field of the pulse. This coherence is destroyed by phase relaxation originating, e.g., from collisions among the carriers, among excitons, or from phonon scattering. The physics of coherent interband polarizations has been studied in both bulk and low-dimensional semiconductors by means of nonlinear optical techniques like temporally and spectrally resolved four-wave mixing, giving insight into the nature of transient polarizations and into many-body effects of the carriers.[2]

Much less is known on the specific shape of the nonequilibrium carrier distribution created by optical excitation, in particular with femtosecond pulses. In the simplest approximation, the initial carrier distribution is determined by the band structure of the semiconductor, i.e., the dispersion of the optically coupled states in **k** space, and by the spectral envelope of the laser pulses. This picture, which considers carrier generation a fully incoherent process, is the basis of many theoretical calculations relying on the Boltzmann equation for the description of ultrafast carrier dynamics. Until now, most simulations using ensemble Monte Carlo (EMC) techniques followed this approach. On the other hand, femtosecond coherent experiments demonstrate that coherent interband polarizations and their dephasing occur on a sub-100-fs time scale, i.e., transiently during carrier generation, and thus cannot be neglected for a correct description of the photogeneration process.[3–5] Theoretical calculations based on the semiconductor Bloch equations predict a substantial broadening of the carrier generation rate compared to the pulse spectrum by dephasing during the excitation pulse.[6–8]

The experimental investigation of this problem requires a technique that gives insight into carrier distributions occurring on a femtosecond time scale. Band-to-acceptor (BA) luminescence in p-type III–V semiconductors represents such a probe, allowing the direct measurement of transient electron distributions.[9–19] The emission is due to recombination of electrons created by continuous wave, picosecond, or femtosecond excitation with holes bound to acceptor atoms. The substantial width of the acceptor wave function in **k** space and the time-independent hole distribution allow a selective observation of the electron dynamics, even at energies high above the band gap and for excitation densities as low as 10^{13} cm^{-3}.

Very recently, we provided direct experimental evidence that the coherent coupling of femtosecond laser pulses with the interband polarization of a semiconductor has strong in-

fluence on the shape of the initial nonequilibrium electron distributions.[19] The transient electron distributions were monitored via BA luminescence and both the width of the luminescence peaks and their dependence on carrier density point to a strong broadening of the distribution by dephasing processes during the excitation pulse. In this paper, we present more detailed studies on nonequilibrium electrons in GaAs under different excitation conditions, namely continuous-wave, picosecond, or femtosecond generation in a wide range of carrier densities. In each case, broadening of the initial distribution due to dephasing processes and inelastic carrier–carrier scattering occurs at different densities, pointing to the different strength of the screened Coulomb interaction in the carrier system. The carrier distributions generated with femtosecond excitation show the fastest spreading in energy. The experimental results are analyzed in detail by theoretical calculations based on a Monte Carlo solution of the semiconductor Bloch equations. The calculation shows that the broadening of the distribution function due to dephasing processes stems mainly from the carrier generation process whereas dephasing during BA recombination makes a minor contribution. Furthermore, the intensity ratio of BA luminescence versus band-to-band (BB) luminescence is calculated and compared to the experimental results.

The paper is organized as follows. After a short description of the experimental techniques in Sec. II, the results of the different experiments are presented in Sec. III. In Sec. IV, we discuss the theoretical approach allowing a solution of the semiconductor Bloch equations with Monte Carlo techniques and present simulations of our experiments. The numerical results are compared to those from a semiclassical treatment in terms of the Boltzmann equation. The relative intensities of BA and BB luminescence and the different contributions to the linewidth in the BA emission spectra are considered in some detail. The discussion in Sec. V is devoted to a comparison of experiment and theory. A brief summary is given in Sec. VI.

II. EXPERIMENTAL TECHNIQUES

In the experiments, a 3-μm-thick p-type GaAs layer grown by molecular beam epitaxy is studied at a lattice temperature of $T_L=10$ K. The sample is doped with Be acceptors of a binding energy of 28 meV (Ref. 20) and (compared to previous experiments on band-to-acceptor luminescence) a relatively low concentration of 3×10^{16} cm^{-3}.[21]

The sample was excited with a home-built Ti:sapphire laser which was operated either in continuous-wave (cw) or self-mode-locked mode at a photon energy of 1.73 eV. The spectral width of the cw output was less than 1 meV. In mode-locked operation, 20 ps pulses of a bandwidth of about 4 meV or bandwidth-limited 150-fs pulses (spectral width 10 meV) were generated, depending on the alignment of the four-prism sequence in the laser cavity.

The luminescence from the GaAs sample was collected with a high-aperture lens system and focused onto the entrance slit of a double monochromator (spectral resolution 1 meV). The spectrally selected intensity was detected with a single-photon counting multiplier with a dark count rate of about 1 s^{-1}.

The excitation densities given below are estimated from the spot size of the laser beam on the sample, the penetration depth, and the number of photons absorbed per pulse. In the different measurements, the sample was oriented under the Brewster angle in the incoming laser beam in order to minimize the reflected intensity and thus the uncertainty in estimating the absorbed photon flux.

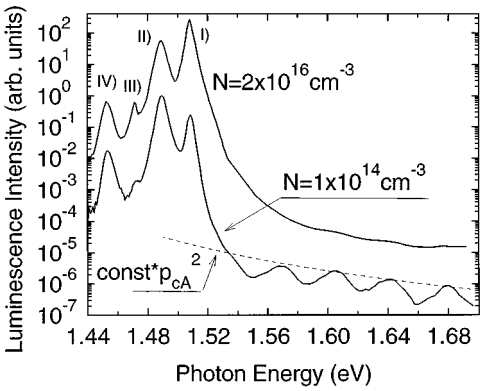

FIG. 1. Total emission spectrum of the p-GaAs sample measured with femtosecond excitation of $N=10^{14}$ and 2×10^{16} electron–hole pairs per cm^3. At low photon energies, we observe luminescence peaks due to recombination of thermalized electrons with free holes (I) and with bound holes (II). The peaks at lower energies originate from recombination processes of electrons with free holes (III) and bound holes (IV) involving simultaneous emission of a photon and an optical phonon. The emission at high photon energies is caused by band-to-acceptor recombination of nonequilibrium electrons (peak structure) and by a very weak background due to band-to-band recombination. The dashed line represents the square of the energy-dependent matrix element p_{cA} of the band-to-acceptor transition.

III. EXPERIMENTAL RESULTS

In our experiments, the excitation energy was 1.73 eV. At this spectral position, transitions from the heavy hole to the conduction band dominate the absorption, whereas transitions from the light hole to the conduction band make a contribution of less than 30%. As a result, the excitation creates predominantly electrons and heavy holes with respective excess energies of $E_e=185$ meV and $E_{hh}=25$ meV. In Fig. 1, we present overall luminescence spectra recorded after femtosecond excitation of 10^{14} and 2×10^{16} electron-hole pairs per cm^3, respectively. The emission intensity is plotted on a logarithmic scale as a function of photon energy. We find intense emission at photon energies between 1.44 and about 1.52 eV which is related to different recombination channels of thermalized electrons that populate states in the Γ minimum of the conduction band. Peak I is due to the recombination of those electrons with free holes created by the excitation pulse whereas peak II located below the band gap is related to recombination with holes bound to the acceptors. Peaks III and IV at even lower photon energy originate from the corresponding processes in which a photon and an optical phonon are emitted simultaneously upon recombination.

For our study of ultrafast carrier dynamics, we concentrate on the very weak high-energy tail of emission which is dominated by the recombination of nonequilibrium electrons

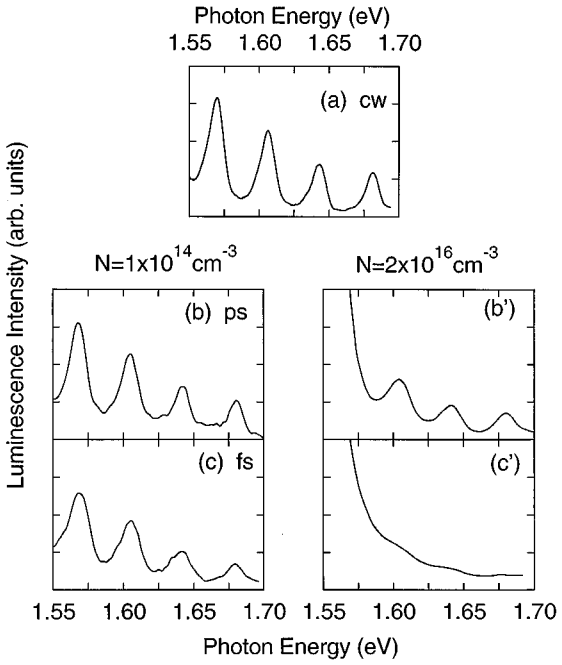

FIG. 2. Spectra of band-to-acceptor luminescence from p-type GaAs at a temperature of $T_L=10$ K for different excitation conditions. The spectra were measured with (a) continuous wave, (b) 20 ps, and (c) 150-fs excitation of $N_{ex}=10^{14}$ electrons per cm^3 (photon energy 1.73 eV). Parts (b′) and (c′) give results for $N_{ex}=2\times10^{16}$ cm^{-3}.

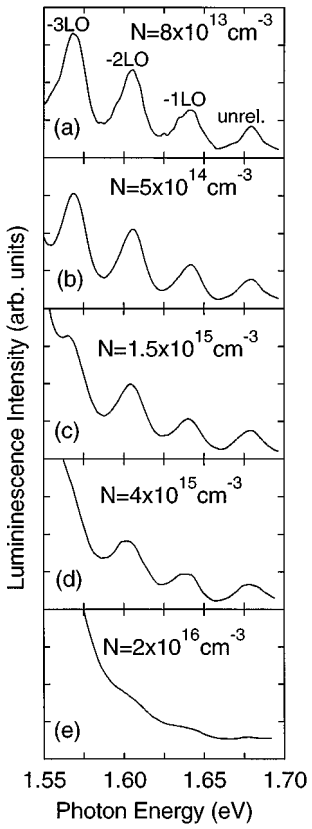

FIG. 3. (a)–(e) Hot electron luminescence spectra of GaAs (lattice temperature $T_L=10$ K) measured for different carrier densities N that are generated by femtosecond excitation. The intensity of band-to-acceptor emission is plotted versus photon energy. The spectra show a first peak (unrel.) that originates from conduction band states optically coupled by the excitation pulse (photon energy 1.73 eV, pulse duration 150 fs), and a series of phonon replicas. Within the experimental accuracy, the lines exhibit an identical spectral width and broaden with increasing carrier concentration.

with bound holes. Recombination of electrons and photogenerated holes, i.e., the band-to-band transition, makes a much smaller contribution as will be discussed below. Owing to the acceptor binding energy and the dispersion of the valence band, the BA emission is red-shifted with respect to the excitation at 1.73 eV and exhibits—for low densities—a series of well-pronounced luminescence lines, separated from each other by roughly the energy of a LO phonon. Electrons directly excited by the laser pulse give rise to the peak at the highest photon energy of 1.68 eV, whereas the lines at lower energy, the so-called phonon replicas, are due to carriers that have emitted one, two, or three LO phonons. The relative peak intensities of the individual luminescence lines follow quite well the square of the energy-dependent matrix element p_{cA} of the band-to-acceptor transition (dashed line). In particular, the intensity of the lower peaks increases mainly because of the rising matrix element.[22] At a carrier concentration of 2×10^{16} cm^{-3}, the different peaks are strongly broadened, resulting in a nearly structureless high-energy tail of emission.

In Fig. 2, we present emission spectra for two different carrier densities created by (a) continuous-wave excitation or by (b,b′) 20 ps, and (c,c′) 150 fs pulses. The spectral width ΔE of the different lines in each spectrum is identical within the experimental accuracy. The absolute value of ΔE is similar for continuous-wave and picosecond excitation, whereas a substantially higher linewidth is found for femtosecond excitation. The linewidth increases with density as is obvious from the data of the right column of Fig. 2. It is important to note that the line structure of the spectra disappears at lower carrier density for femtosecond excitation than for picosecond generation. This behavior is related to carrier–carrier scattering in the distinctly different photogenerated electron distributions[15,23] and will be discussed below. The change of the spectra with carrier density is shown in more detail in Fig. 3 for femtosecond generation. We present data for five different excitation densities.

For femtosecond excitation, the spectral profile of the first peak was studied in detail. Spectra were recorded up to a photon energy of 1.695 eV. At higher energies, the suppression of stray light from the excitation pulse was not sufficient to isolate the very weak luminescence. In Fig. 4, the first emission peak is plotted for three carrier concentrations on an extended energy scale and compared to the (redshifted) spectral profile of the laser pulses (solid line). In all cases, the spectral width of the BA peaks is considerably higher than the pulse width of about 10 meV.

In Fig. 5(a), the linewidth of the first peak is plotted as a function of density for picosecond (circles) and femtosecond excitation (squares). Both sets of data show a strong increase of linewidth on different density scales. In Fig. 5(b), the spectral width of the first three luminescence peaks which are separated in time by a single LO phonon emission time $\tau_{LO}=160$ fs, is plotted for an excitation density of 4×10^{15} cm^{-3}. The first (‘‘unrelaxed’’) peak exhibits almost the same

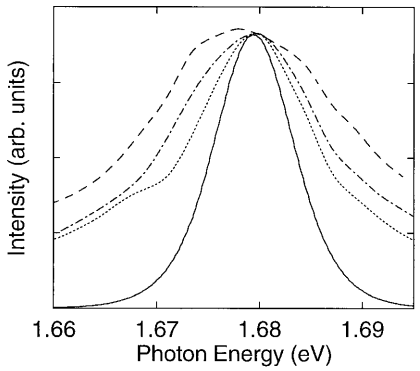

FIG. 4. Spectral profile of the first luminescence peak for carrier densities of $N=8\times10^{13}$ cm^{-3} (dotted line), 5×10^{14} cm^{-3} (dash-dotted line), and 4×10^{15} cm^{-3} (dashed line). For comparison, the spectral envelope of the femtosecond excitation pulses is shown (shifted to lower photon energy by 50 meV, solid line).

spectral width as the phonon replicas occurring at later times. The same behavior is found in the picosecond measurements [Fig. 5(c), carrier density 4×10^{16} cm^{-3}].

IV. THEORETICAL CALCULATIONS

A. Carrier generation process

On the semiclassical level the generation and scattering dynamics of photoexcited carriers is described by the Boltzmann equation (BE) for the distribution functions of electrons (f^e_k) according to

$$\frac{d}{dt} f^e_{\mathbf{k}} = g_{\mathbf{k}}(t) - \sum_{\mathbf{k}'} [W^e_{\mathbf{k}'\mathbf{k}} f^e_{\mathbf{k}} (1-f^e_{\mathbf{k}'}) - W^e_{\mathbf{k}\mathbf{k}'} f^e_{\mathbf{k}'} (1-f^e_{\mathbf{k}})], \tag{1}$$

where the generation rate $g_{\mathbf{k}}(t)$ and the scattering rates $W^e_{\mathbf{k}'\mathbf{k}}$, describing a scattering process from state $\mathbf{k}$ to $\mathbf{k}'$, are calculated from Fermi's golden rule. The generation rate is, except for the energy dispersion of the optically coupled states and for transient phase space filling effects, fully determined by the temporal and spectral characteristics of the laser pulse. The dynamics of the distribution function of holes ($f^h_{\mathbf{k}}$) is described by an analogous Boltzmann equation with the same generation rate and scattering rates $W^h_{\mathbf{k}'\mathbf{k}}$. On this level all effects related to the coherence of the laser pulse are neglected. The coherent dynamics in semiconductors, on the other hand, is described by the semiconductor Bloch equations (SBE) which involve, besides the distribution functions, also the interband polarization $p_{\mathbf{k}}$. Treating scattering processes in the semiclassical limit, the polarization dynamics is given by

$$\frac{d}{dt} p_{\mathbf{k}} = \frac{1}{i\hbar} [(\epsilon^e_{\mathbf{k}} + \epsilon^h_{\mathbf{k}}) p_{\mathbf{k}} + M_{\mathbf{k}} E_0(t) e^{-i\omega t} (1 - f^e_{\mathbf{k}} - f^h_{-\mathbf{k}})] - \sum_{\mathbf{k}'} [W^p_{\mathbf{k}'\mathbf{k}} p_{\mathbf{k}} - W^p_{\mathbf{k}\mathbf{k}'} p_{\mathbf{k}'}]. \tag{2}$$

Here, $M_{\mathbf{k}}$ is the dipole matrix element, $E_0(t)$ is the temporal shape of the electric field strength of the laser pulse with frequency ω, $\epsilon^{e,h}_{\mathbf{k}}$ denote the single-particle energies of electrons and holes, and c.c. denotes complex conjugate.[24] The scattering part in Eq. (2) has the same structure as in Eq. (1). The corresponding matrices are related to the scattering rates of electrons and holes according to

$$W^p_{\mathbf{k}'\mathbf{k}} = \frac{1}{2} \sum_{\nu=e,h} [W^\nu_{\mathbf{k}'\mathbf{k}} (1-f^\nu_{\mathbf{k}'}) + W^\nu_{\mathbf{k}'\mathbf{k}} f^\nu_{\mathbf{k}'}], \tag{3}$$

reflecting the fact that scattering processes of both electrons and holes lead to a dephasing of the polarization. The dynamics of the distribution functions is again described by Eq. (1), the generation rate, however, being calculated according to

$$g_{\mathbf{k}} = \frac{1}{i\hbar} [M_{\mathbf{k}} E_0(t) e^{-i\omega t} p^*_{\mathbf{k}} - \text{c.c.}]. \tag{4}$$

The generation rate [Eq. (4)] involves the interband polarization which is influenced by the density-dependent scattering processes entering Eq. (2) and therefore, in contrast to the semiclassical case, the generation rate becomes density dependent.

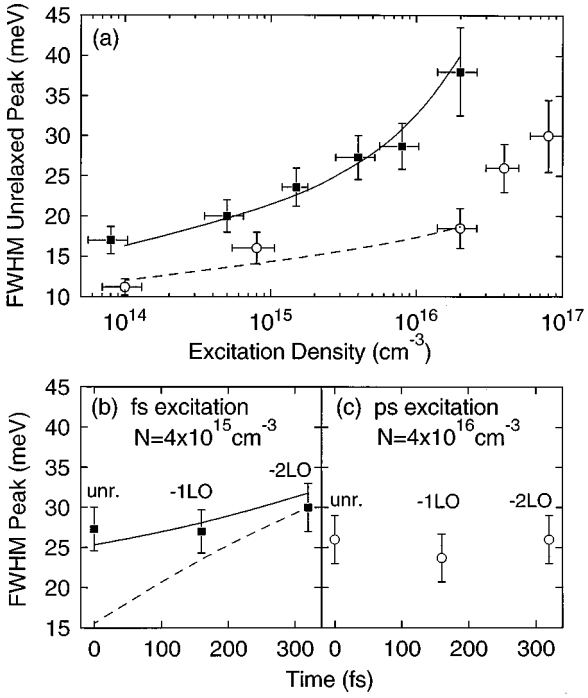

FIG. 5. Spectral full width at half-maximum (FWHM) of the first luminescence peak (unrel.) as a function of carrier density for picosecond (circles) and femtosecond excitation (squares). The femtosecond data are compared to theoretical values calculated from a simulation including the coherent coupling of femtosecond pulses and polarization in the sample (solid line) and from a semiclassical model of the incoherent carrier dynamics (dashed line). (b) Spectral width of the first, second (−1LO), and third (−2LO) luminescence peak for femtosecond excitation (carrier density 4×10^{15} cm^{-3}). The solid line was calculated from the simulation based on the semiconductor Bloch equations, the dashed line represents the semiclassical result. The time scale was calculated with an LO phonon emission time of 160 fs. (c) Spectral width of the luminescence peaks measured with picosecond excitation (carrier concentration 4×10^{16} cm^{-3}).

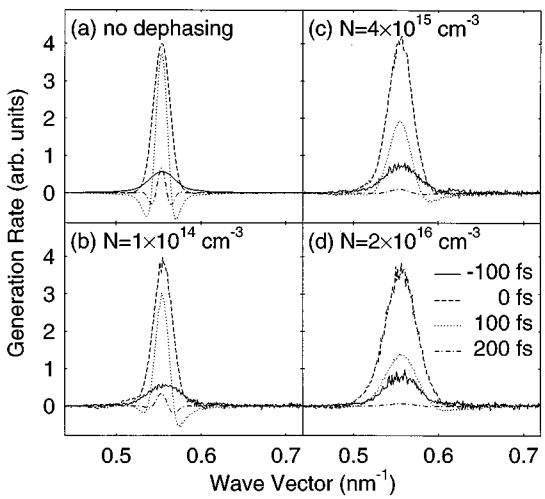

FIG. 6. Generation rate of electrons as a function of wave vector at different times as calculated from the semiconductor Bloch equations (a) without any dephasing processes and (b)–(d) including dephasing due to carrier–carrier and carrier–phonon scattering for densities of (b) 10^{14} cm^{-3}, (c) 4×10^{15} cm^{-3}, and (d) 2×10^{16} cm^{-3}. Time zero represents the maximum of the 150-fs excitation pulse.

The second term in the sum of Eq. (2) which has the structure of an in-scattering term, is often neglected on the basis of a random phase argument because it involves a summation over the complex polarization components at different wave vectors. Then, the scattering part for $p_{\mathbf{k}}$ reduces to the common structure $[\propto -p_k/T_2(\mathbf{k})]$ with a $\mathbf{k}$-dependent dephasing time T_2. However, it turns out that a correct modeling of the dephasing including the in-scattering term is crucial to obtain a physically reasonable density dependence of the dynamics.[25] In particular at low densities, where mainly small-angle processes occur in carrier-carrier scattering, there is a strong cancellation between in- and out-scattering terms and the total scattering rate T_2 leads to a strong overestimation of the dephasing which results, e.g., in very broad and clearly unphysical generation rates.

To compare the different models of carrier dynamics in photoexcited semiconductors the BE and the SBE were solved numerically for the experimental conditions of bulk GaAs excited by a 150-fs laser pulse at 1.73 eV. The band structure considered in the calculations consists of a parabolic heavy hole valence band (effective mass $m_{hh}=0.45m_0$, m_0 free electron mass) and the conduction band ($m_e=0.063m_0$).[8,25] Other material parameters used for the solution of the BE and SBE have been summarized in Table I of Ref. 7. The BE was solved by a standard ensemble Monte Carlo (EMC) simulation including both carrier–carrier and carrier–phonon scattering. The treatment of Coulomb interaction in the carrier system uses static screening with a time-dependent screening length that is up-dated according to the changes in the carrier distribution. The solution of the SBE is based on a combined technique including a generalized Monte Carlo simulation for the incoherent part of both distribution functions and polarization and a direct integration of the coherent part of the equations.

In Fig. 6, the generation rate at different times as obtained from the SBE is plotted as a function of wave vector. Figure 6(a) shows the result obtained if no scattering processes are taken into account ($W^p_{\mathbf{k}'\mathbf{k}}=0$). The time dependence can be understood as follows:[7] Energy-time uncertainty leads to an initially very broad generation rate; with increasing time the line narrows and, in the tails, exhibits negative parts due to a stimulated recombination of carriers initially generated off-resonance. After the pulse, the distribution function of the generated carriers is in good agreement with the BE result using a Gaussian spectral profile of the generation rate the shape of which is time independent. For the rates shown in Figs. 6(b)–6(d) carrier–carrier and carrier–phonon scattering processes as described by the matrices $W^{e,h,p}_{\mathbf{k}'\mathbf{k}}$ have been taken into account. In contrast to the semiclassical generation rate, a strong density dependence is observed. At the lowest density the behavior is essentially the same as in the case without scattering. With increasing density carrier–carrier scattering processes become more efficient. Scattering processes destroy the coherence between electrons and holes which is necessary for the stimulated recombination processes. As a consequence the negative tails are strongly reduced with increasing density and the generation remains broad for all times resulting in a much broader carrier distribution than in the BE case.

The main feature of the SBE approach is a broadening of the generation process. Thus, the question arises as to whether this broadening could be simply included in an incoherent BE approach which would considerably reduce the computer time for the simulations. However, there is no simple way of directly obtaining this broadening from the distribution functions. The total scattering rate leads to a strong overestimation of the spectral width and—furthermore—the lineshape derived from the SBE is non-Lorentzian. This originates from the cancellation between in- and out-scattering contributions in the polarization equation. The only way to obtain an approximate result in the BE approach is to perform a matrix inversion at each time step which, however, is not much simpler than solving the SBE.

B. Luminescence line shape

The luminescence which serves for monitoring the carrier dynamics is based on the same light–matter interaction mechanism as the carrier generation process. Therefore, radiative recombination processes should be influenced by scattering processes in the same way as the photogeneration process discussed above, resulting in an additional density-dependent broadening of the spectrum. However, there is a big quantitative difference between BB and BA luminescence as will be discussed in the following. Our theoretical treatment shows that the broadening of the BA luminescence is negligible compared to the broadening associated with carrier generation.

In contrast to the coherent generation by a laser pulse where the light field is treated classically, the luminescence is due to spontaneous emission, requiring a quantum mechanical treatment of the photon field.[7,26] A complete theory of the broadening of BB and BA luminescence spectra will be published elsewhere.[27] Here we will concentrate on the main aspects and the physical origin of the differences between both types of spectra.

The broadening of a luminescence transition is determined by the scattering part of the respective polarization.

For band-to-band transitions it is given by the scattering matrices in Eq. (2). Thus, as expected, the broadening of the BB luminescence transition is the same as the broadening of the generation process. This situation changes, however, when looking at band-to-acceptor transitions which are described by an electron–acceptor polarization $p^a_{\mathbf{k}}$. The quantum mechanical calculation where the Coulomb interaction between electrons in the conduction band and in acceptor states has to be taken into account, leads to a scattering part for the electron–acceptor polarization according to

$$\left.\frac{d}{dt}\,p^a_{\mathbf{k}}\right|_{\text{scat}} = -\sum_{\mathbf{k}'}\,[W^a_{\mathbf{k}'\mathbf{k}}p^a_{\mathbf{k}} - \beta_{|\mathbf{k}-\mathbf{k}'|}W^a_{\mathbf{k}\mathbf{k}'}p^a_{\mathbf{k}'}], \qquad (5)$$

where $\beta_q=[1+(qa_B/2)^2]^{-2}$ is the Fourier transform of the charge density in the acceptor state, a_B is the acceptor Bohr radius, and the scattering matrix is given by

$$W^a_{\mathbf{k}'\mathbf{k}} = \tfrac{1}{2}[W^e_{\mathbf{k}'\mathbf{k}}(1-f^e_{\mathbf{k}'}) + W^e_{\mathbf{k}'\mathbf{k}}f^e_{\mathbf{k}'}]. \qquad (6)$$

The dephasing dynamics of $p^a_{\mathbf{k}}$ is characterized by two main differences with respect to $p_{\mathbf{k}}$. First, due to the factor β_q there is no more complete symmetry between in- and out-scattering terms. However, for q values smaller than the inverse Bohr radius, which are the dominant scattering terms at low densities, this symmetry is fulfilled approximately and the general features related to the in-scattering terms which have been found for the interband case still hold. Second, and more important, the scattering matrix is determined only by scattering processes of electrons which is due to the fact that free holes are not involved in such transitions.

Because of the complexity of the problem a full time-dependent quantum-kinetic calculation of the luminescence spectrum has not yet been performed. However, we can analyze the importance of the broadening by looking at the spectrum produced by fixed carrier distributions generated by a 150-fs pulse and ignoring any relaxation of the carrier distributions after the pulse. We have calculated the line shape of BB and BA luminescence spectra by a numerical matrix inversion[7] involving the scattering matrices $W^p_{\mathbf{k}'\mathbf{k}}$ and $W^a_{\mathbf{k}'\mathbf{k}}$ due to carrier–carrier interaction for distribution functions obtained from a BE and a SBE generation rate.

In Fig. 7, BB and BA luminescence spectra are shown for different models at densities of 10^{14} [Fig. 7(a), (a′)] and 2×10^{16} cm^{-3} [Fig. 7(b), (b′)]. In a semiclassical treatment, generation and recombination do not lead to any additional broadening and the width of the spectra is determined by the energetic width of the electron distribution, i.e., by the laser spectrum (dash-dotted lines). In contrast, the SBE approach fully accounts for dephasing processes during the generation, giving rise to an additional density-dependent broadening as discussed above. The dashed lines show the corresponding spectra if no additional broadening of the luminescence transition is taken into account. Considering exclusively the broadening upon recombination, i.e., the intrinsic emission linewidth, we get the dotted lines in Fig. 7. For BB luminescence we find a somewhat larger broadening of the luminescence than of the generation since the efficiency of carrier–carrier scattering processes during generation increases with density and the dephasing is gradually built up, while the broadening of the luminescence is completely determined by the final carrier density. We observe very broad spectra at high density [Fig. 7(b)] which are caused by the very high scattering rates of free holes in the valence band. A completely different behavior is observed for band-to-acceptor luminescence. Here, the broadening during recombination of electrons with bound holes of negligible scattering rate is quite small even at the highest density [Fig. 7(b′), dotted line], resulting in a profile of the emission line close to the semiclassical calculation. As a consequence, when taking into account the broadening due to both generation and recombination processes (solid lines in Fig. 7), the BB transition exhibits a broadening with similar contributions from generation and recombination, whereas the width of the BA line originates predominantly from the generation process. This result justifies the use of a semiclassical model to describe the BA recombination in the dynamic calculations discussed in the following.

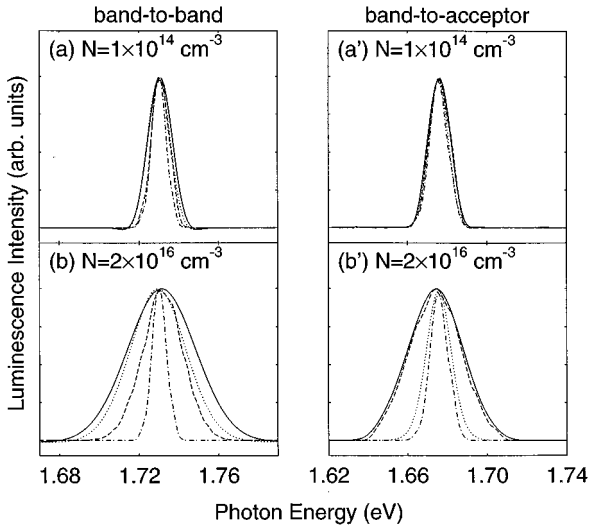

FIG. 7. Calculated spectral profiles of luminescence due to band-to-band- and band-to-acceptor recombination for carrier concentrations of (a), (a′) 10^{14} cm^{-3} and (b), (b′) 2×10^{16} cm^{-3}. A carrier distribution generated by a 150-fs pulse is considered. The dash-dotted lines were calculated from a semiclassical model using a golden rule approach for the generation and recombination rate. For the dashed lines, the broadening of the generation process was taken into account while the recombination rate was calculated from the golden rule. The dotted lines were obtained with a golden rule generation rate and using a broadened recombination rate. The solid lines give the result when broadening of both generation and recombination processes are included. For band-to-acceptor luminescence, the broadening of the recombination process is negligible.

C. Spectra of band-to-acceptor luminescence

The theoretical framework outlined above was used to calculate the spectra of band-to-acceptor luminescence for a variety of experimental parameters. In Fig. 8, we present results for femtosecond excitation calculated from the semiclassical approach [Figs. 8(a)–(e)] and from the SBE treatment [Figs. 8(a′)–(e′)]. Several pronounced differences are found between the two calculations. In the semiclassical model, the unrelaxed (first) peak marked bold in the figure is clearly visible up to the highest density of 2×10^{16} cm^{-3}

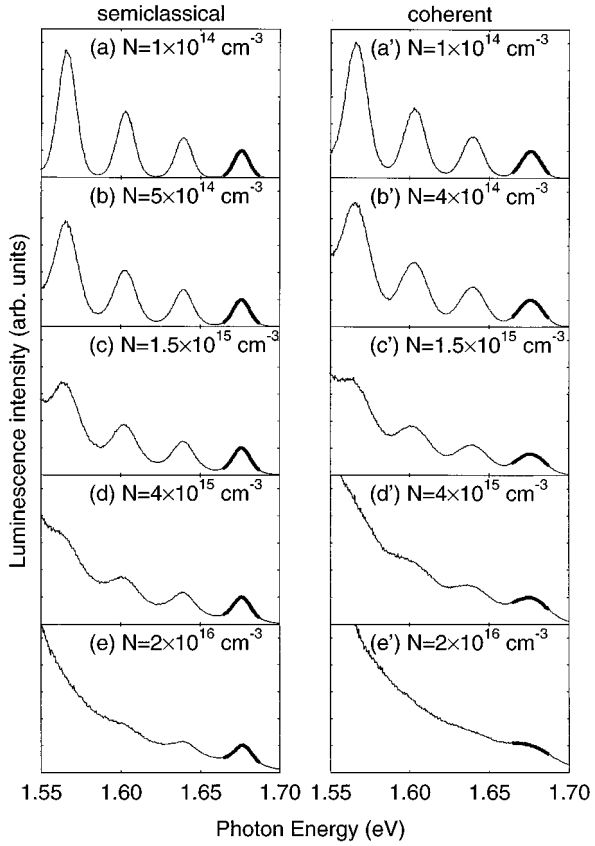

FIG. 8. Luminescence spectra calculated for femtosecond excitation from the simulations of (a)–(e) the semiclassical Boltzmann equation (BE) and (a′)–(e′) the semiconductor Bloch equations (SBE, same parameters as in the experiment). At higher carrier densities [(d) and (e)], the BE results show an increase of the spectral width of successive luminescence lines. In contrast, the SBE results give nearly identical widths of all lines for a fixed density. The marked regions emphasize the different behavior of the unrelaxed peak for the two models.

while the coherent (SBE) model gives a strongly broadened peak. The FWHM of this peak as a function of density is plotted in Fig. 5(a) for the coherent (solid line) and the semiclassical (dashed line) model, together with the experimental results. The semiclassical spectra calculated for elevated densities [Figs. 8(d)–(e)] exhibit an increase in the broadening of subsequent peaks which is nearly absent in the SBE calculations and in the experimental results. To demonstrate this difference more quantitatively, the full width at half-maximum of the three first peaks of the spectrum at a density of 4×10^{15} cm^{-3} is plotted in Fig. 5(b) for the coherent (solid line) and the semiclassical (dashed line) model.

For the case of picosecond excitation a quantitative comparison with the experimental results has not been performed for two reasons: First, an excitation with a 20-ps pulse requires a simulation of the dynamics over at least 50 ps compared to typically about 3 ps in the case of femtosecond excitation resulting in an increase in CPU time by a factor of more than 15 and, second, for the simulation of the SBE the time dependence of the electric field of the laser pulse is needed including detailed knowledge of the chirp which is not available. However, in order to study the trends observed in the experiments and to investigate the role of the polarization dynamics in the case of longer pulses, we have performed simulations for an excitation with a 1.8-ps (transform-limited) pulse.

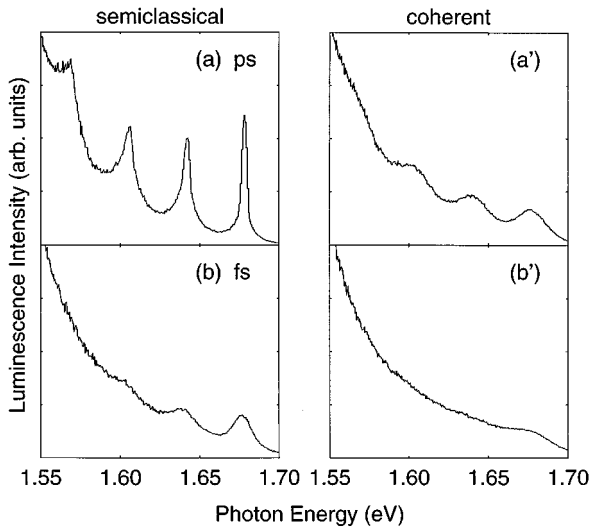

FIG. 9. Luminescence spectra calculated for an excitation (a), (a′) with a 1.8-ps pulse and (b), (b′) with a 150-fs pulse from the simulations of (a), (b) the semiclassical Boltzmann equation and (a′), (b′) the semiconductor Bloch equations at a density of 2×10^{16} cm^{-3}. In the picosecond case the broadening of the peaks is much weaker due to the increase in the screening wave vector resulting in a reduced scattering and dephasing efficiency.

In Fig. 9, the resulting luminescence spectra obtained from the semiclassical and the coherent model at a density of 2×10^{16} cm^{-3} are compared with the corresponding spectra for excitation with a 150-fs pulse. For both models we find the general behavior that the spectra are narrower in the case of excitation with a longer pulse, as is also confirmed by the experiment (Fig. 2). However, in this case the deviations between the semiclassical and the coherent model are much more pronounced. The reason is that in the semiclassical model the width of the generation is determined by the spectral width of the laser, which decreases with increasing pulse duration, while in the coherent model the time which determines the width is given by the minimum of pulse duration and dephasing time, the latter being the relevant quantity in the present case. The semiclassical spectra exhibit a pronounced increase in the broadening of subsequent peaks in contrast to the coherent results where for both excitation conditions a negligible increase is observed.

It should be noted that for picosecond excitation, in particular when using the semiclassical model, the effects of warping and broadening of the acceptor level result in a considerable additional broadening of the spectra. However, this broadening is density independent in contrast to the broadening due to dephasing processes. Figure 9 shows that at densities above 10^{16} cm^{-3} dephasing makes a substantial contribution to the broadening of the peaks.

D. Band-to-band luminescence

Finally we want to address a phenomenon which cannot be avoided in the experiments. Electrons do not only recombine with bound holes at the acceptors but also with free

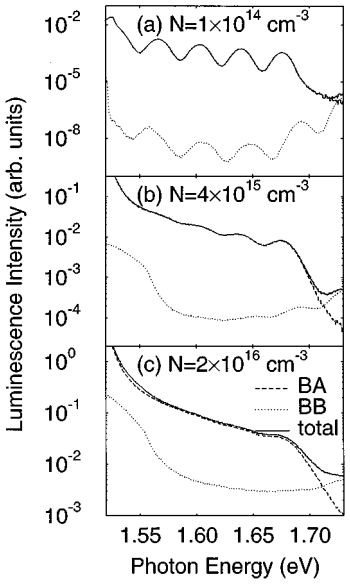

FIG. 10. Calculated spectra of band-to-acceptor (dashed lines), band-to-band (dotted lines), and total (solid lines) luminescence occurring after femtosecond excitation of (a) 10^{14}, (b) 4×10^{15}, and (c) 2×10^{16} electrons per cm^3. The luminescence intensity is plotted on a logarithmic scale versus photon energy. For photon energies in the range between 1.55 and 1.70 eV, the band-to-band intensities are much lower than those of the band-to-acceptor luminescence.

holes in the valence band. This results in a background in the spectra caused by band-to-band (BB) recombination. In order to estimate the magnitude of this background for our experimental conditions, we have calculated also the BB luminescence spectrum in the coherent model. The results are shown in Fig. 10 on a logarithmic intensity scale. We find that at the lowest density the BB intensity in the relevant energy range is more than four orders of magnitude smaller than the BA spectrum. With increasing density this background increases, however, even at the highest density it is still one order of magnitude weaker. As a consequence, it has negligible influence on the shape of the peaks observed in BA luminescence.

V. DISCUSSION

In the following, we first discuss the carrier generation and the recombination processes for femtosecond excitation and their influence on the emission spectra. This part is followed by a comparative analysis of the data taken with femtosecond and with picosecond excitation.

In our experiments, the 150-fs excitation pulse creates carriers on a time scale that is somewhat shorter than the emission time of LO phonons of about 160 fs. At low carrier densities (10^{14} cm^{-3}), the redistribution of electrons due to Coulomb scattering is slower than LO phonon emission and, consequently, the majority of electrons is part of the nonequilibrium distribution that gives rise to the first (unrelaxed) peak in the BA spectrum. The peaks at lower photon energy derive from this first maximum by emission of single LO phonons (phonon replicas). They are emitted at later times. Our results in Figs. 2–5 reveal the following important features. (i) With increasing excitation density, the spectral width of the luminescence peaks increases strongly, leading to more or less smooth emission spectra at high density. The peak structure disappears at carrier concentrations around 2×10^{16} cm^{-3} for femtosecond excitation, whereas the picosecond data show structure up to about 10^{17} cm^{-3} (see, for comparison, also Ref. 11). (ii) The luminescence spectra taken with femtosecond excitation at densities below 10^{15} cm^{-3} show a spectral width of the first emission peak of 17 to 20 meV, significantly higher than the bandwidth of the 150-fs laser pulses of 10 meV (Fig. 4). The inhomogeneous broadening due to warping of the valence band which makes a density-independent contribution of 8–10 meV cannot account for this excess linewidth.[13] (iii) The femtosecond data taken in a wide range of carrier density from 10^{14} up to 2×10^{16} cm^{-3} demonstrate that the spectral width of the different lines, i.e., the unrelaxed peak and the replicas, is identical within each spectrum.

From the viewpoint of a semiclassical description, this behavior is interpreted in the following way.[11,16–18] The laser pulse generates an initial nonequilibrium distribution of electrons with an energetic width that is determined by the spectral width of the pulse and by band-structure details like heavy-hole warping. The latter contribution has been well characterized in cw measurements of BA luminescence and makes a density-independent contribution to the overall linewidth. With increasing carrier density, the rates of inelastic Coulomb scattering increase, leading to a spreading of the electron distribution over a wider energy range and, thus, to a broadening of the luminescence peaks. The spreading rates of the distribution depend on the effective Coulomb interaction among the carriers. Different numbers have been reported, depending on the specific type of screening that was used in the calculations.[16] With respect to the BA luminescence spectra, this picture predicts a broadening of the emission peaks that increases with time. Thus, starting from the unrelaxed peak, the spectral width of the luminescence peaks should increase continuously, i.e, phonon replicas at lower energies should exhibit a width larger than those at higher energies and, in particular, larger than the unrelaxed peak. The spectra calculated with a conventional (semiclassical) EMC simulation [Figs. 5 and 8(a)–(c)] show exactly this behavior. The width of the calculated luminescence peaks plotted in Fig. 5(b) (dashed line) show a pronounced increase which remains true even if more refined models of scattering rates, e.g., dynamical screening, or band structure, e.g., warping, are considered.

It is important to note that the semiclassical picture is in strong contrast to our experimental findings. First, for carrier densities $N<10^{15}$ cm^{-3}, theoretical simulations of Coulomb scattering give inelastic carrier–carrier scattering rates much too low to account for the large width of the luminescence peaks observed after femtosecond excitation.[14,16] Second, the experimental spectra show the same spectral width for all luminescence lines. The latter discrepancy demonstrates that the dominant contribution to the linewidth is present already in the unrelaxed peak and originates from the carrier generation process whereas the subsequent redistribution of electrons is of minor importance. The experimental results are fully accounted for by the SBE calculations including the coherent interband polarization and its dephasing. During excitation, the coherent coupling of the laser pulse with the

polarization of the sample gives rise to a nonequilibrium electron distribution that covers a substantially wider energy interval than the spectrum of the transform-limited laser pulses. The spectral width of the carrier generation rate which is shown in Fig. 6 for different times during the pulse and different excitation densities, is determined by a momentary spectral width which corresponds to the inverse of the time elapsed after the onset of the pulse. For an idealized system with dephasing times much longer than the pulse duration, the negative contributions of the generation rate at later times lead to a carrier distribution determined by the pulse spectrum. During the pulse, however, phase-breaking scattering events destroy the coherence, suppress this recombination off-resonance, and result in a width of the distribution which is substantially larger than the energetic width of the laser pulse.

The dephasing of the coherent interband polarization is dominated by the dynamics of free holes which show scattering rates considerably higher than the photoexcited electrons. The carrier generation term and the band-to-band luminescence are sensitive to scattering of free holes and show a strong broadening compared to which the broadening of BA luminescence, i.e., upon recombination with bound holes, is negligible. Thus the width of the luminescence peaks is essentially determined by the width of the generation rate, whereas the contribution of the subsequent intraband scattering of electrons, the only broadening mechanism in the semiclassical model, is of minor importance.

There is a second point related to the details of carrier–carrier scattering which is important for the dominance of dephasing over redistribution. Even if the total carrier–carrier scattering rate is approximately density independent, the decrease in the screening wave vector with decreasing density leads to an increasing number of small-angle scattering processes resulting in a less efficient carrier redistribution and also, as recently pointed out,[8] in a less efficient dephasing. The same argument holds for elastic carrier–impurity scattering. With rising density, the efficiency of carrier–carrier scattering for dephasing starts at lower densities than that for electron redistribution. This behavior is again due to the fact that the decay of the interband polarization is strongly influenced by hole–hole scattering which is much faster than electron–electron scattering.

The spectra calculated from the SBE approach (Fig. 8) are in excellent agreement with the experimental results (Fig. 3). In particular, the relatively large linewidth at low excitation density, the increase of linewidth with density, and the identical width of the different peaks for a fixed density are fully reproduced by the calculation. It is interesting to note that the linewidths observed at densities around 10^{16} cm^{-3} correspond to a dephasing kinetics of the interband polarization on a time scale well below 100 fs, a behavior that has been observed in femtosecond four-wave-mixing experiments with bulk GaAs.[3,4]

The luminescence spectra taken with high carrier densities of 4×10^{15} and 2×10^{16} cm^{-3} show slightly more structure than the calculations of Figs. 8(d′) and 8(e′) performed for the same densities. In the experiment, the Gaussian intensity profile of the femtosecond laser beam results in a small spatial variation of carrier density across the excited spot on the sample. In addition, the experimental error of absolute carrier densities has a relatively large value of about $\pm30\%$. On the other hand, the calculation assumes a spatially homogeneous excitation and gives a strong increase of the luminescence line-width between 3×10^{15} and 2×10^{16} cm^{-3} as displayed in Fig. 5(a). Thus the overall spectra are very sensitive to a spatial variation and the uncertainty of the absolute carrier density, leading to the slight discrepancies between theory and experiment.

A comment should be made on the extraction of linewidths from the luminescence spectra. In a recent publication on BA luminescence generated with femtosecond excitation,[15] a strong background due to BB luminescence[12] was claimed to make a measurement of the linewidth at higher densities impossible. Band-to-band luminescence spectra measured with an undoped GaAs sample were used for a background correction of BA spectra from a *p*-doped sample. It was assumed that—at a density of about 2×10^{16} cm^{-3}—the intensity of the background under the first luminescence maximum (unrelaxed peak) was about 1/4 of the peak intensity. After subtraction, the author found a similar linewidth of the BA luminescence peaks for densities of 10^{15} and 2×10^{16} cm^{-3}.

Unfortunately, the comparison of luminescence intensities from different samples is very difficult because of the different quantum yields of luminescence and, thus, the calibration of BB versus BA intensities shows a large experimental error. The strong background claimed in Ref. 15 is not consistent with the results presented here and in Ref. 19. The data of Fig. 1, which give complete emission spectra for two carrier densities, show a strong decrease of *thermalized* luminescence between 1.52 and 1.56 eV which is due to the strong exponential decrease of the electron and hole populations at larger k values. Extrapolation of this emission to higher photon energies leads to intensities much smaller than claimed in Ref. 15 and completely negligible compared to the BA intensities of Fig. 1. Band-to-band emission from nonthermalized carriers represents a second possible source of background. This contribution can be estimated from the calculated spectra in Fig. 10 where the relative intensities of BA and BB emission are plotted on a logarithmic scale. Even for the highest carrier density, the background under the first and second peak is less than 10% of the BA intensity and can be neglected. This behavior is related to the very efficient thermalization of holes, leading to a very rapid spreading of the initial distribution and a transfer of holes from states at large k vector to states around the maximum of the valence band at $k=0$.[28] Although the rise of the BB spectra towards 1.73 eV gives evidence of some nonthermal hole populations in states directly coupling to the pump pulse at 1.73 eV, the overall emission intensity is much smaller than in BA luminescence. We conclude that the background emission does not affect the extraction of linewidths from the BA spectra.

We now compare the data taken with femtosecond and with picosecond or cw excitation. At the same density, the latter show narrower luminescence lines which is due (i) to the smaller bandwidth of excitation, and, more important, (ii) to lower scattering rates of the photogenerated carriers. For femtosecond excitation, most electrons are concentrated in the nonequilibrium distribution responsible for emission of the first luminescence peak at early times. For picosecond excitation, however, the photogeneration rate of carriers is

much lower than the intraband redistribution rates. Consequently, the majority of electrons form a quasiequilibrium distribution at the bottom of the conduction band and the few electrons which populate the directly excited states at high excess energy and give rise to the hot luminescence, interact with this cold distribution. It has been shown that screening of the Coulomb interaction in such a distribution is much more effective than in the absence of cold carriers at the bottom of the band.[16,23,29] Thus the scattering rates during and after picosecond (cw) excitation are lower, resulting in a slower dephasing kinetics, a smaller broadening of the generation rate, and narrower luminescence lines. For this reason, the peak structure of BA luminescence persists up to higher carrier densities. This behavior is fully confirmed by the calculations.

VI. SUMMARY

In conclusion, we have presented an experimental and theoretical study of band-to-acceptor luminescence under different excitation conditions in order to get insight into the coherent coupling of laser radiation and the interband polarization of GaAs, affecting the electron distributions on the femtosecond and picosecond time scale. Our results demonstrate that dephasing processes during photogeneration lead to a strong broadening of the initial carrier distribution that shows an energetic width larger than the femtosecond excitation pulses. The emission spectra, in particular the identical width of the unrelaxed peak and the different phonon replicas, demonstrate that—for femtosecond excitation—this mechanism is much more important than the redistribution of electrons by inelastic carrier–carrier scattering. An analysis of the recombination process shows that broadening upon band-to-acceptor recombination is negligible compared to the broadening of the generation rate. These results demonstrate the dominant role of coherent effects for luminescence generated by femtosecond excitation.

For picosecond or continuous-wave excitation, narrower emission lines are found that persist up to higher carrier densities. This behavior is mainly due to the different carrier distribution in which stronger screening of the Coulomb interaction results in lower scattering rates among the carriers and, thus, less efficient dephasing and redistribution. This interpretation is supported by the excellent agreement of our experimental data with the results from a Monte Carlo solution of the semiconductor Bloch equations.

ACKNOWLEDGMENTS

We thank S. Haas and W. Kaiser for valuable discussions. One of us (T. K.) wishes to thank the Deutsche Forschungsgemeinschaft for financial support within the framework of the Sonderforschungsbereich 296.

[1] For a recent overview see Hot Carriers in Semiconductors, Proceedings of the 8th International Conference, edited by J. F. Ryan and A. C. Maciel [Semicond. Sci. Technol. **9** (5S) (1994)].

[2] For a review see *Coherent Optical Interactions in Semiconductors*, edited by R. T. Phillips (Plenum, New York, 1994).

[3] P. C. Becker, H. L. Fragnito, C. H. BritoCruz, R. L. Fork, J. E. Cunningham, J. E. Henry, and C. V. Shank, Phys. Rev. Lett. **61**, 1647 (1988).

[4] A. Lohner, K. Rick, P. Leisching, A. Leitenstorfer, T. Elsaesser, T. Kuhn, F. Rossi, and W. Stolz, Phys. Rev. Lett. **71**, 77 (1993).

[5] J. L. Oudar, D. Hulin, A. Migus, A. Antonetti, and F. Alexandre, Phys. Rev. Lett. **55**, 2074 (1985).

[6] T. Kuhn and F. Rossi, Phys. Rev. Lett. **69**, 977 (1992).

[7] T. Kuhn, and F. Rossi, Phys. Rev. B **46**, 7496 (1992).

[8] F. Rossi, S. Haas, and T. Kuhn, Phys. Rev. Lett. **72**, 152 (1994).

[9] D. N. Mirlin, I. Ja. Karlik, L. P. Nikitin, I. I. Reshina, and V. F. Sapega, Solid State Commun. **37**, 757 (1981).

[10] R. G. Ulbrich, J. A. Kash, and J. C. Tsang, Phys. Rev. Lett. **62**, 949 (1989).

[11] J. A. Kash, Phys. Rev. B **40**, 3455 (1989); **47**, 1221 (1993).

[12] J. A. Kash, and J. C. Tsang, Solid State Electron. **31**, 419 (1988).

[13] G. Fasol, W. Hackenberg, H. P. Hughes, K. Ploog, E. Bauser, and H. Kano, Phys. Rev. B **41**, 1461 (1990).

[14] D. W. Snoke, W. W. Rühle, Y.-C. Lu, and E. Bauser, Phys. Rev. Lett. **68**, 990 (1992); Phys. Rev. B **45**, 10 979 (1992).

[15] J. A. Kash, Phys. Rev. B **51**, 4680 (1995).

[16] J. F. Young, N. L. Henry, and P. J. Kelly, Solid State Electron. **32**, 1567 (1989).

[17] M. G. Kane, K. W. Sun, and S. A. Lyon, Semicond. Sci. Technol. **9**, 697 (1994).

[18] K. W. Sun, M. G. Kane, and S. A. Lyon, Europhys. Lett. **26**, 123 (1994).

[19] A. Leitenstorfer, A. Lohner, T. Elsaesser, S. Haas, F. Rossi, T. Kuhn, W. Klein, G. Boehm, G. Traenkle, and G. Weimann, Phys. Rev. Lett. **73**, 1687 (1994).

[20] D. J. Ashen, P. J. Dean, D. T. J. Hurle, J. B. Mullin, and A. M. White, J. Chem. Solids **36**, 1041 (1975).

[21] For the moderate doping level of the sample, the splitting of the acceptor ground state is less than 4 meV as determined from band-gap-related luminescence, i.e., the line shapes of the hot luminescence are not influenced by this effect.

[22] W. P. Dumke, Phys. Rev. **132**, 1998 (1963).

[23] J. F. Young, T. Gong, P. M. Fauchet, and P. J. Kelly, Phys. Rev. B **50**, 2208 (1994).

[24] Coulomb renormalizations of the carrier energies and the external field are taken into account in the calculations. However, they are not important under the conditions studied here. For details see Ref. 7.

[25] T. Kuhn, S. Haas, and F. Rossi, Phys. Status Solidi B **188**, 417 (1995).

[26] J. Schilp, T. Kuhn, and G. Mahler, Phys. Rev. B **50**, 5435 (1994).

[27] T. Kuhn (unpublished).

[28] T. Elsaesser, J. Shah, L. Rota, and P. Lugli, Phys. Rev. Lett. **66**, 1757 (1991).

[29] L. Rota, P. Poli, C. Jacoboni, and P. Lugli, in *Proceedings of the 20th International Conference on the Physics of Semiconductors*, edited by E. Anastassakis and J. D. Joannopoulos (World Scientific, Singapore, 1990), p. 2534.